Mechanics of Advanced Materials and Structures
Publication details, including instructions for authors and subscription information:
http://www.tandfonline.com/loi/umcm20

Buckling of Functionally Graded Cylindrical Shells under Combined Loads

Huaiwei Huang [a], Qiang Han [a b], Nengwen Feng [a] & Xuejun Fan [a]

[a] Department of Engineering Mechanics, South China University of Technology, Guangzhou, PR China

[b] College of Architectural and Civil Engineering, Xinjiang University, Urumqi, PR China

Available online: 04 Jul 2011

To cite this article: Huaiwei Huang, Qiang Han, Nengwen Feng & Xuejun Fan (2011): Buckling of Functionally Graded Cylindrical Shells under Combined Loads, Mechanics of Advanced Materials and Structures, 18:5, 337-346

To link to this article: http://dx.doi.org/10.1080/15376494.2010.516882

Mechanics of Advanced Materials and Structures, 18:337–346, 2011

ISSN: 1537-6494 print / 1537-6532 online
DOI: 10.1080/15376494.2010.516882

Taylor & Francis
Taylor & Francis Group

Buckling of Functionally Graded Cylindrical Shells under Combined Loads

Huaiwei Huang,[1] Qiang Han,[1,2] Nengwen Feng,[1] and Xuejun Fan[1]

[1]*Department of Engineering Mechanics, South China University of Technology, Guangzhou, PR China*
[2]*College of Architectural and Civil Engineering, Xinjiang University, Urumqi, PR China*

By using the Ritz energy method and finite element method, buckling behaviors of combined-loaded functionally graded cylindrical shells are investigated. The combined loads are composed of axial, lateral, and torsional loads. Results show that the contribution of lateral pressure to buckling is more significant than that of axial compression or torsion and the contributions of axial compression and torsion are almost the same. Also, a practical method is proposed in this article to determine the load-dominant bound between the single buckling mode due to one dominant load and the mixed buckling mode due to interaction of the two loads.

Keyword FGMs, cylindrical shells, combined-load, buckling, energy method, FEM

1. INTRODUCTION

Functionally graded materials (FGMs) are a kind of new material, born in 1984 [1], and usually made from a mixture of two constituents, i.e., ceramic and metallic materials. The volume fractions of these constituents vary continually through FGMs' thickness, which enables a smooth change in material properties. Thus, there are at least two advantages. First, because of the smooth change in the material properties of FGMs, stress concentration seen commonly in the disconnected material interfaces of the traditional fiber-reinforced or laminated composites can be effectively released. Second, optimization design of internal stresses can be easily achieved by altering the distribution of their constituents.

Early attention had been paid to thermoelastic and thermoinelastic characters of FGM structures [2–7]. Recently, stability problems of FGMs, such as their vibration and buckling behaviors, have attracted more and more attention. Loy et al. [8] and Bhangale and Ganesan [9] studied free vibration characters of functionally graded cylindrical shells (FGCSs). Also, force vibration of axially period-loaded FGCSs was discussed by Ng et al. [10] and Darabi et al. [11]. Buckling stability of FGCSs is another important research field deserved to be focused on. By using the first shear deformation theory and the Donnell theory, respectively, Shahsiah and Eslami [12] and Wu et al. [13] considered the effects of various temperature distributions on thermal buckling of FGCSs. However, Shahsiah never included the thermal conduction effect, while Wu never considered the temperature-dependent material properties of FGMs. Taking both into account, Kadoli et al. [14] dealt with the same problem and revealed some valuable results for thermal buckling and vibration characters of FGCSs. Li and Batrab [15] and Najafizadeh et al. [16] presented linear buckling analyses for middle-layered and stiffened FGCSs under axial load, respectively. Sofiyev [17, 18] and Sofiyev and Schnack [19] studied dynamic buckling behaviors of FGCSs under time-dependent torsional, lateral, and axial loads.

Except for the linear static or dynamic buckling of FGCSs, using the boundary layer theory, Shen [20, 21] and Shen and Noda [22] presented a series of systematical analyses for postbuckling behaviors of FGCSs under axial and lateral loads as well as their combination. Although his theory included simultaneously the effects of nonlinear prebuckling deformations, the postbuckling large deflections, and initial geometric imperfections, the complicated formulation restricted its applications.

Generally, in-served cylindrical shells usually buckle not merely under one of the basic loads, i.e., axial compression, lateral pressure, and torsion, but under a combination of them. Fundamental theoretical and experimental studies on combined-loaded isotropic cylindrical shells had been systematically reported by Yamaki [23]. Also, Shen [24] and Shen and Xiang [25] presented theoretical analyses for laminated cylindrical shells under axial-lateral and axial-torsional combined-loads. However, investigation on buckling of combined-loaded FGCSs was seldom touched. In this article, buckling behaviors of combined-loaded FGCSs are investigated by using two different methods: the Ritz energy method and FEM. Three combined load cases were considered, including axial-lateral, axial-torsional, and lateral-torsional combined-loads. The effects of various

Received 28 November 2008; accepted 19 October 2009.
Address correspondence to Qiang Han, Department of Engineering Mechanics, South China University of Technology, Guangzhou 510640, PR China. E-mail: emqhan@scut.edu.cn

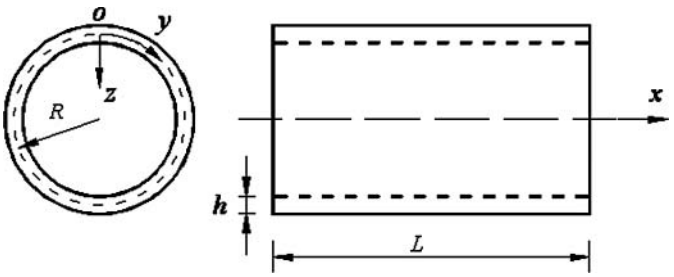

FIG. 1. Geometry and coordinate system of FGCSs.

combined-loads on buckling of FGCSs are discussed at length. Meanwhile, a practical method is proposed in this article to determine the load-dominant bound between the single buckling mode due to one dominant load and the mixed buckling mode due to interaction of the two loads.

2. FORMULATIONS

Figure 1 shows a FGCS with length l, mean radius R, and thickness h. The origin o is located on the left end and at the middle plane of the shell. x, y, and z are in the axial, circumferential, and inner normal directions, respectively.

2.1. Material of FGMs

FGMs are inhomogeneous materials generally made from a mixture of ceramic and metallic constituents. Generally, the volume fraction of the ceramic material is assumed to follow a power law distribution according to Reddy and Chin [5].

$$V_c = (0.5 + z/h)^N, \; V_c + V_m = 1, \tag{1}$$

where V_c and V_m denotes, respectively, the volume fractions of the ceramic and metallic constituents, and N is the power law exponent or the inhomogeneous parameter. The material property of FGMs P_f is given as:

$$P_f = P_m V_m + P_c V_c, \tag{2}$$

where P_c and P_m are the material properties of ceramic and metallic constituents. From Eqs. (1) and (2), P_f can be rewritten as:

$$P_f(z) = P_m + (0.5 + z/h)^N (P_c - P_m). \tag{3}$$

Herein, P_f can be used to represent FGMs' material properties, such as Young's modulus E_f, Poisson ratio μ_f, etc., and we have:

$$\begin{aligned} E_f(z) &= E_m + (0.5 + z/h)^N (E_c - E_m) \\ \mu_f(z) &= \mu_m + (0.5 + z/h)^N (\mu_c - \alpha_m). \end{aligned} \tag{4}$$

2.2. Basic Equations

The constitutive relations of cylindrical shells are

$$\begin{Bmatrix} \sigma_x \\ \sigma_y \\ \tau_{xy} \end{Bmatrix} = \begin{bmatrix} Q_{11} & Q_{12} & 0 \\ Q_{21} & Q_{22} & 0 \\ 0 & 0 & Q_{66} \end{bmatrix} \begin{Bmatrix} \varepsilon_x \\ \varepsilon_y \\ \gamma_{xy} \end{Bmatrix}, \tag{5}$$

where $Q_{11} = Q_{22} = E_f(z)/(1-\mu_f^2)$, $Q_{12} = \mu_f E_f(z)/(1-\mu_f^2)$, $Q_{66} = E_f(z)/\left[2\left(1+\mu_f\right)\right]$, and the strain components $\{\varepsilon\}$ are given as:

$$\{\varepsilon\} = \begin{Bmatrix} \varepsilon_x \\ \varepsilon_y \\ \gamma_{xy} \end{Bmatrix} = \begin{Bmatrix} \varepsilon_x^0 + zk_x \\ \varepsilon_y^0 + zk_y \\ \gamma_{xy}^0 + zk_{xy} \end{Bmatrix}. \tag{6}$$

Based on Von-Kárman nonlinear strain-displacement relation, the strain components $\{\varepsilon^0\}$ and the curvature components $\{k\}$ on the reference surface are

$$\left\{\varepsilon^0\right\} = \begin{Bmatrix} \varepsilon_x^0 \\ \varepsilon_y^0 \\ \gamma_{xy}^0 \end{Bmatrix} = \begin{Bmatrix} u_{,x} \\ v_{,y} - w/R \\ u_{,y} + v_{,x} \end{Bmatrix}, \tag{7}$$

$$\{k\} = \begin{Bmatrix} k_x \\ k_y \\ k_{xy} \end{Bmatrix} = -\begin{Bmatrix} w_{,xx} \\ w_{,yy} \\ 2w_{,xy} \end{Bmatrix}, \tag{8}$$

in which $u(x, y)$, $v(x, y)$, and $w(x, y)$ are the displacements along x, y, and z axes, respectively. Subscripts following a comma stand for partial differentiations.

For thin cylindrical shells with $h/R << 1$, the approximate forms of internal force and moment resultants are

$$\{(N_x, N_y, N_{xy}), (M_x, M_y, M_{xy})\} = \int_{-\frac{h}{2}}^{\frac{h}{2}} \{\sigma_x, \sigma_y, \tau_{xy}\}(1, z) dz. \tag{9}$$

Substitution of Eq. (5) into Eq. (9) obtains:

$$\begin{Bmatrix} N \\ M \end{Bmatrix} = \begin{bmatrix} A & B \\ B & D \end{bmatrix} \begin{Bmatrix} \varepsilon^0 \\ k \end{Bmatrix} \quad \text{or} \quad \begin{Bmatrix} \varepsilon^0 \\ M \end{Bmatrix} = \begin{bmatrix} A^* & B^* \\ C^* & D^* \end{bmatrix} \begin{Bmatrix} N \\ k \end{Bmatrix}, \tag{10}$$

where

$$\begin{aligned} [N, M]^T &= [N_x, N_y, N_{xy}, M_x, M_y, M_{xy}]^T, \\ A^* &= A^{-1}, B^* = -A^{-1}B, D^* = D - BA^{-1}B, C^* \\ &= -(B^*)^T, \\ A_{ij} &= \int_{-\frac{h}{2}}^{\frac{h}{2}} Q_{ij} dz, B_{ij} \\ &= \int_{-\frac{h}{2}}^{\frac{h}{2}} Q_{ij} z dz, D_{ij} = \int_{-\frac{h}{2}}^{\frac{h}{2}} Q_{ij} z^2 dz, (i, j = 1, 2, 6). \end{aligned}$$

The strain energy of a thin cylindrical shell is approximated to be

$$U = \frac{1}{2}\iiint_V (\sigma_x\varepsilon_x + \sigma_y\varepsilon_y + \tau_{xy}\varepsilon_{xy})dV, \tag{11}$$

where V represents the volume field of the shell. With the aid of Eqs. (6) and (9), the above equation is rewritten as:

$$\begin{aligned} U &= \frac{1}{2}\iint_S (N_x\varepsilon_x^0 + N_y\varepsilon_y^0 + N_{xy}\gamma_{xy}^0)dxdy \\ &+ \frac{1}{2}\iint_S (M_xK_x + M_yK_y + M_{xy}K_{xy})dxdy, \end{aligned} \tag{12}$$

where S represents the $x-y$ area field of the shell. The first and the second integrals represent the strain energy, respectively, aroused by membrane forces and bending moments.

The work done by external forces

$$\begin{aligned} W &= N_{x0}\iint_F \left(-\frac{1}{2}w_{,x}^2\right)dxdy + N_{y0}\iint_F \left(-\frac{1}{2}w_{,y}^2\right)dxdy \\ &+ N_{xy0}\iint_F \left(-w_{,x}w_{,y}\right)dxdy \end{aligned} \tag{13}$$

where N_{x0}, N_{y0}, and N_{xy0} are the prebuckling axial, circumferential, and shear membrane forces.

The total potential energy of the system can be written as:

$$\Pi = U - W. \tag{14}$$

From Eq. (7), the compatible equation is obtained as:

$$\varepsilon_{x,yy}^0 + \varepsilon_{y,xx}^0 - \gamma_{xy,xy}^0 = -w_{,xx}/R. \tag{15}$$

Introducing Airy's stress function $F(x, y)$ satisfying

$$N_x = F_{,yy},\ N_y = F_{,xx},\ N_{xy} = -F_{,xy}. \tag{16}$$

With the aid of Eqs. (10) and (16), Eq. (15) becomes:

$$\begin{aligned} &A_{11}^*F_{,yyyy} + \left(2A_{12}^* + A_{66}^*\right)F_{,xxyy} \\ &\quad + A_{22}^*F_{,xxxx} = B_{12}^*\left(w_{,xxxx} + w_{,yyyy}\right) \\ &\quad + \left(2B_{66}^* - B_{11}^* - B_{22}^*\right)w_{,xxyy} - w_{,xx}/R \end{aligned} \tag{17}$$

3. SOLUTION

Assume that the combined-loaded FGCS is approximately simply supported and the deflection is in the following form [26]:

$$w(x, y) = w_0 + w_1 = A_0h + A_1h\sin\frac{m\pi x}{l}\sin\frac{n}{R}(y + \gamma x), \tag{18}$$

where $w_0 = A_0h$ denotes the equivalent prebuckling uniform deflection and $w_1 = A_1h\sin\frac{m\pi x}{l}\sin\frac{n}{R}(y+\gamma x)$ the buckling deflection. A_0, A_1 are unknown amplitude parameters. m, n are the axial half-wave numbers and the circumferential wave numbers, respectively. γ is the included angle between the buckling shape and x-axis.

Herein, the prebuckling deflection is assumed to be uniform to simplify the formulation. In fact, the prebuckling deflection w_0 is always much smaller than the buckling one w_1 and negligible in buckling analysis, so this assumption would not affect the accuracy of the buckling prediction. Other than the prebuckling deflection, the buckling deflection w_1 satisfies the simple support boundary conditions in the integral sense.

For convenience, Eq. (18) is written as:

$$w(x, y) = A_0h + \frac{1}{2}A_1h\left[\cos\frac{n}{R}(y + jx) - \cos\frac{n}{R}(y + kx)\right], \tag{19}$$

where $j = \gamma - \bar{\theta}$, $k = \gamma + \bar{\theta}$, and $\bar{\theta} = m\pi R/(nl)$.

Substituting Eq. (19) into Eq. (17), one obtains:

$$\begin{aligned} F(x, y) &= a\cos\frac{n}{R}(y + jx) + b\cos\frac{n}{R}(y + kx) + \frac{1}{2}N_{y0}x^2 \\ &+ \frac{1}{2}N_{x0}y^2 - N_{xy0}xy, \end{aligned} \tag{20}$$

where

$$a = \frac{A_1hRj^2}{2n^2\left(1 + j^2\right)^2A_{11}^*}b = -\frac{A_1hRk^2}{2n^2\left(1 + k^2\right)^2A_{11}^*}.$$

From force boundary conditions,

$$\begin{aligned} &\int_0^{2\pi R} N_{x0}dy + h\int_0^{2\pi R} pdy = 0,\ R\int_0^{2\pi R} N_{xy0}dy + Rh \\ &\int_0^{2\pi R} Sdy = 0, \end{aligned} \tag{21}$$

and one obtains:

$$N_{x0} = -ph,\ N_{y0} = -qR,\ N_{xy0} = -Sh \tag{22}$$

It is convenient to define the nondimensional parameters as:

$$p_1 = pA_{11}^*R,\ p_2 = qA_{11}^*R^2/h,\ \tau = SA_{11}^*R,\ \eta = n^2h/R$$

Considering Eqs. (19) and (20) in Eqs. (12) and (13), one obtains the total potential energy from Eq. (14):

$$\begin{aligned}\Pi &= \frac{A_1^2 h^2 l\pi}{4A_{11}^* R}\left\{\left[\frac{j^4}{\left(1+j^2\right)^2}+\frac{k^4}{\left(1+k^2\right)^2}\right]\right.\\ &\quad -\eta\left[(j^2+k^2)p_1+2p_2+2(j+k)\tau\right]\\ &\quad \left.+\frac{D_{11}^* A_{11}^* \eta^2}{h^2}\left[(j^2+1)^2+(k^2+1)^2\right]\right\}\\ &\quad +\frac{h^2 l\pi}{A_{11}^* R}\left[p_1^2+p_2^2-2\mu p_1 p_2+2(1+\mu)\tau^2\right]. \quad (23)\end{aligned}$$

Applying the Ritz energy method, $\frac{\partial \Pi}{\partial A_1}=0$, and noting $A_1 \neq 0$, one obtains:

$$\begin{aligned}&\frac{j^4}{\left(1+j^2\right)^2}+\frac{k^4}{\left(1+k^2\right)^2}+\frac{D_{11}^* A_{11}^* \eta^2}{h^2}\left[(1+j^2)^2+(1+k^2)^2\right]\\ &\quad -\eta\left[p_1\left(j^2+k^2\right)+2p_2+2\tau(j+k)\right]=0.\end{aligned} \quad (24)$$

This equation can be used to derive the buckling condition of combined-loaded FGCSs.

Considering a pure axial compression case with $\gamma=0$, one obtains from Eq. (24):

$$ph=\frac{1}{A_{11}^* R^2}\left(\frac{\alpha}{\alpha^2+\beta^2}\right)^2+D_{11}^*\left(\frac{\alpha^2+\beta^2}{\alpha}\right)^2 \quad (25)$$

where $\alpha=m\pi/l$, $\beta=n/R$. Minimizing p with regard to $\frac{\alpha}{\alpha^2+\beta^2}$ yields the axial critical load:

$$p_{cr}=2\sqrt{D_{11}^*/A_{11}^*}/(Rh) \quad (26)$$

which can easily be further degraded to the classical critical load of isotropic ceramic shells,

$$p_{cr}=E_c h/\left(R\sqrt{1-\mu_c^2}\right)$$

when $N=0$

In a pure lateral pressure case with $\gamma=0$, from Eq. (24), the lateral critical load is

$$qR=\frac{\alpha^2}{\beta^2}\left(\frac{1}{A_{11}^* R^2}\left(\frac{\alpha}{\alpha^2+\beta^2}\right)^2+D_{11}^*\left(\frac{\alpha^2+\beta^2}{\alpha}\right)^2\right). \quad (27)$$

This equation can easily be degraded to that of an isotropic shell by setting $N=0$, that is,

$$qR=E_c h\left[\frac{\alpha^4}{R^2\beta^2\left(\alpha^2+\beta^2\right)^2}+\frac{h^2(\alpha^2+\beta^2)^2}{12\beta^2(1-\mu_c^2)}\right], \quad (28)$$

with $qR=\sigma_{0y}h$ (where σ_{0y} denotes the average hoop stress), Eq. (28) is equivalent to that obtained from the classical linear theory [27].

In a pure torsional load case and from Eq. (24), we have

$$\begin{aligned}Sh &= \frac{1}{4R^2\beta^2\gamma A_{11}^*}\left\{\frac{(\alpha-\beta\gamma)^4}{\left[\beta^2+(\alpha-\beta\gamma)^2\right]^2}+\frac{(\alpha+\beta\gamma)^4}{\left[\beta^2+(\alpha+\beta\gamma)^2\right]^2}\right.\\ &\quad \left.+2R^2 A_{11}^* D_{11}^*\left[\alpha^4+\beta^4(1+\gamma^2)^2+2\alpha^2\beta^2(1+3\gamma^2)\right]\right\}\end{aligned} \quad (29)$$

In a pure load case, from Eqs. (25), (28), and (29), the corresponding critical load p_{cr}, q_{cr}, and S_{cr} can be derived by minimizing p, q, and S with regard to various values of m, n, as well as γ in the case of torsion. Similarly, in a combined load case, one can determine the parameters of the critical load p_{1cr}, p_{2cr}, and τ_{cr} from Eq. (24). For example, giving the value of p_1, p_2, one obtains τ_{cr} by minimizing τ with regards to various values of m, n, and γ.

4. ANALYTICAL RESULTS

The FGMs discussed in this article are chosen to be a mixture of silicon nitride and stainless steel (or Si_3N_4/SUS304). The Young's modulus of these two constituents are $E_c = 322.27GPa$, $E_m = 207.79GPa$, and FGMs' Poisson ratio $\mu_f = 0.28$.

4.1. Verification of the Present Theory

To verify the present theory, comparisons made with Shen [21] in Table 1 for laterally loaded homogeneous cylindrical shells indicate a maximal derivation of the critical load less than 3%. In addition, the buckling modes consist very well with those in the literature. Meanwhile, the reproduced data from Sofiyev's formulations [17–19] on the static critical axial, lateral, and torsional loads of FGCSs are compared in Table 2.

4.2. Analytical Results

Three two-load combination cases, i.e., axial and lateral combined-load case (ALCC), axial and torsional combined-load case (ATCC), and lateral and torsional combined-load case (LTCC) are considered in the present work.

Figures 2–4 (with the calculating parameters listed) plot the relation curves of the corresponding critical load parameter p_{1cr}, p_{2cr}, or τ_{cr} versus the power law exponent N under the three two-load combination cases with one of the loads fixed. All of the critical load parameters decrease rapidly and then increase slowly with the increase of N. From Figures 2a and 2b it can be seen that p_{1cr} decreases greatly with the increase of p_2, while p_{2cr} decreases slightly with the increase of p_1. From Figures 3a and 3b it is shown that p_{1cr} decreases with the increase of τ, and τ_{cr} decreases with the increase of p_1. From Figures 4a and 4b it can be seen that p_{2cr} keeps nearly invariable

TABLE 1
Verification of the present critical lateral load q_{cr} ($\times 10^{-4}$ MPa) of homogeneous cylindrical shells

L/R	R/h	Shen [21]	Present	Difference (%)
0.5	300	2761.397 (1, 15)[a]	2809.31 (1, 16)	1.74
	3000	7.8184 (1.28)	7.94526 (1, 29)	1.62
1	300	1272.597 (1, 11)	1294.65 (1, 11)	1.73
	500	348.588 (1, 13)	353.781 (1, 13)	1.49
	1000	60.5364 (1, 15)	61.3375 (1, 15)	1.32
	1500	21.7969 (1, 17)	21.9684 (1, 17)	0.79
	2000	10.5690 (1, 18)	10.6375 (1, 18)	0.65
	3000	3.8144 (1, 20)	3.83065 (1, 20)	0.43
2	300	611.7448 (1, 8)	617.626 (1, 8)	0.96
	3000	1.8842 (1, 14)	1.89097 (1, 14)	0.36
3	300	402.6016 (1, 7)	413.996 (1, 7)	2.83
	3000	1.2511 (1, 12)	1.25669 (1, 12)	0.45
5	300	239.0987 (1, 5)	239.831 (1, 5)	0.31
	3000	0.7482 (1, 9)	0.748563 (1, 9)	0.05

[a]The numbers in the parentheses denote the buckling mode (m, n).

TABLE 2
Comparison of the critical loads (in MPa) of FGCSs with those reproduced from Sofiyev (Si_3N_4/SUS304, $R/h = 500$, $L/R = 2$)

	Si_3N_4	$N = 0.2$	$N = 0.5$	$N = 1$	$N = 2$	$N = 5$	$N = 10$	$N = 20$	SUS304
The critical axial load p_{cr}									
Sofiyev [19]	387.631	362.064	338.303	316.927	297.936	279.100	268.659	261.018	249.933
Present	387.631	361.612	337.604	316.294	297.745	279.521	268.970	261.163	249.933
The critical lateral load q_{cr}									
Sofiyev [17]	0.0262	0.0243	0.0228	0.0215	0.0203	0.0191	0.0184	0.0178	0.0169
Present	0.0272	0.0252	0.0235	0.0221	0.0209	0.0198	0.0191	0.0185	0.0175
The critical torsional load S_{cr}									
Sofiyev [18]	73.721	68.465	64.178	59.990	56.912	53.412	51.394	49.859	47.533
Present	74.224	69.044	64.381	60.404	57.139	53.978	51.950	50.325	47.857

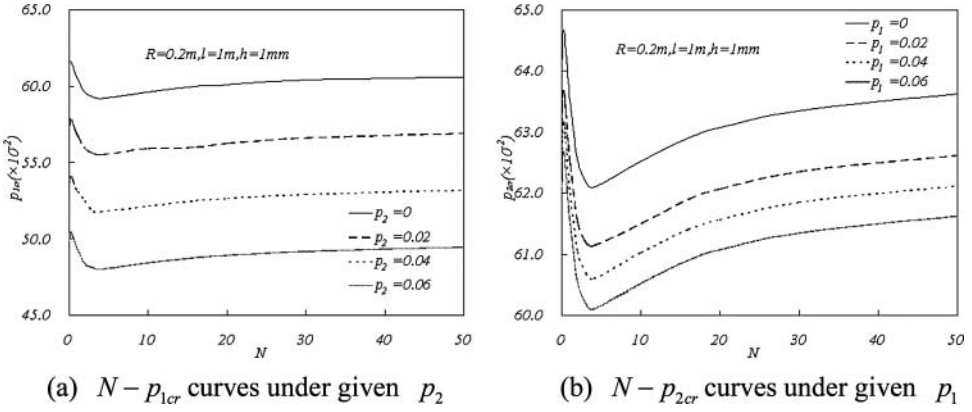

(a) $N - p_{1cr}$ curves under given p_2 (b) $N - p_{2cr}$ curves under given p_1

FIG. 2. Relation curves of the critical parameters versus the power law exponent under ALCC.

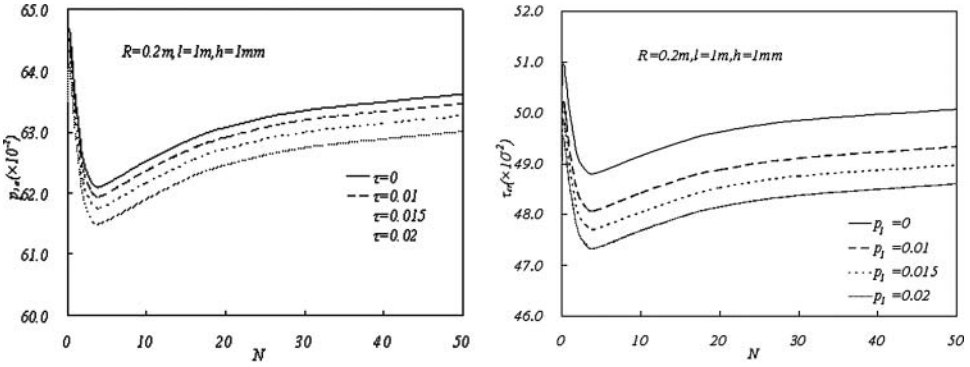

(a) $N-p_{1cr}$ curves under given τ (b) $N-\tau_{cr}$ curves under given p_1

FIG. 3. Relation curves of the critical parameters versus the power law exponent under ATCC.

and decreases slightly with the increase of τ, and τ_{cr} decreases markedly with the increase of p_2.

5. FEM RESULTS

FEM is one of the most effective methods to solve complicated engineering problems. It is also effective in solving eigenvalue problems of buckling. However, due to absence of a ready material option in the existing FEM codes, it is difficult in simulating FGMs' material properties, which vary smoothly through the thickness. For this reason, there is still no precise modeling of FGMs by the FEM code in the literature. Some studies, with regard to three-dimensional elastic analysis by ANSYS code, were reported by Yang et al. [28] and Liu [29]. They regarded FGMs as multilayer materials and define the material properties of each layer as an isotropic one. This kind of modeling method easily leads to imprecise modeling of FGMs' material properties and complication in modeling treatment.

Due to absence of a ready material option in the existing FEM codes, in this article, the FORTRAN code helps to form the stiffness matrix of FGMs' shell element, which can be input into the general FEM code ABAQUS through its UMAT module. It should be noted that the shear factor of the shell is given as $5/6$ in the present finite element analysis, and the shell is simply supported. The aforementioned Si_3N_4/SUS304 material properties are also used in this section. For the aforementioned three two-load combination cases, load-ratio parameters are introduced as $\lambda_1 = q/p, \lambda_2 = S/p, \lambda_3 = S/q$. Figure 5 shows the finite element model of FGCSs from the ABAQUS code.

5.1. Buckling under Axial and Lateral Combined-Load

Figures 6a–6d show the buckling modes under various load-ratio parameters λ_1 (the basic calculating parameters used are listed in the title of the figures for convenience). It is clear that, with the increase of λ_1, the buckling mode converts gradually from the classical axially loaded buckling mode characterized by $m = 8$ (see Figure 6a) to the classical laterally loaded buckling mode characterized by $m = 1$ (see Figure 6d). The axial half wave number m also decreases with the increase of λ_1. Figures 6b and 6c show mixed buckling modes aroused by interaction between the axial load and the lateral load.

Figure 7 shows excellent agreement between theoretical results and FEM results. It is remarkable that, with the

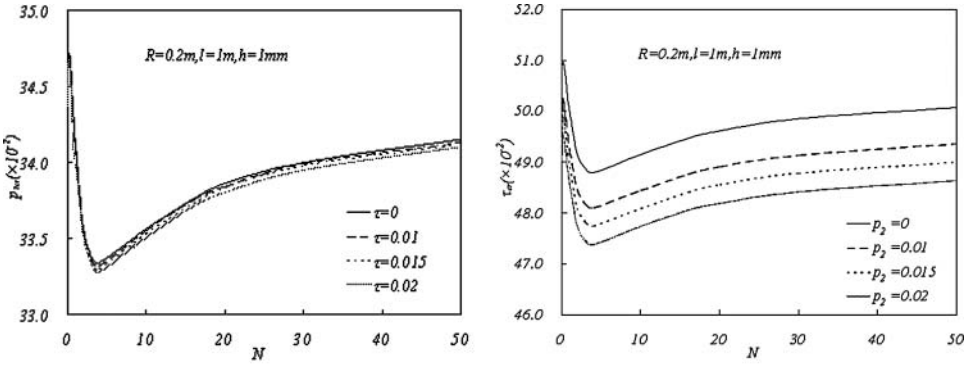

(a) $N-p_{2cr}$ curves under given τ (b) $N-\tau_{cr}$ curves under given p_2

FIG. 4. Relation curves of the critical parameters versus the power law exponent under LTCC.

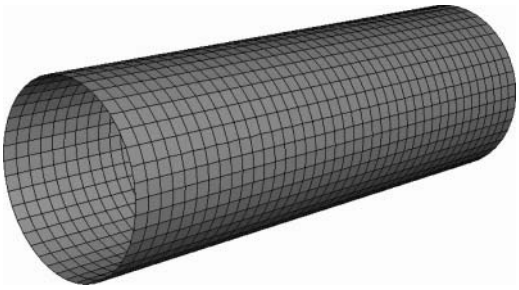

FIG. 5. Finite element model of FGCSs from ABAQUS.

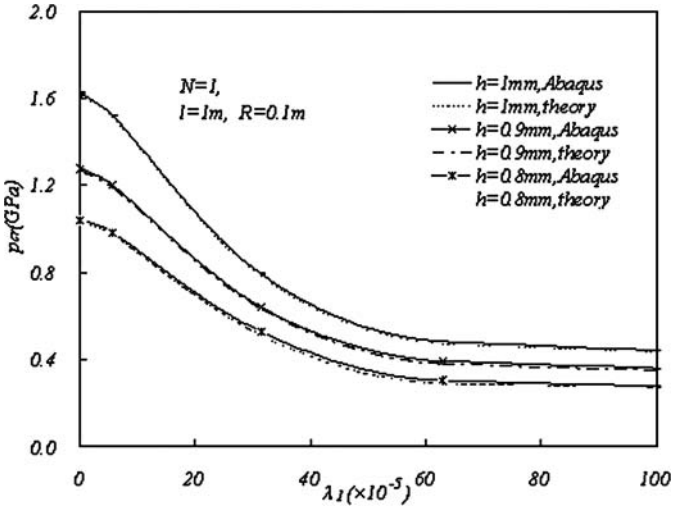

FIG. 7. Comparison of theoretical results with FEM results under ALCC.

increase of λ_1, there appears in order a slow, rapid, and then re-slow decrease of P_{cr}. This shows that buckling of the structure is more sensitive to lateral load than to axial load, and the value of λ_1 can accordingly be divided into three different regions, i.e., $(0, 5 \times 10^{-5})$, $(5 \times 10^{-5}, 30 \times 10^{-5})$, and $[30 \times 10^{-5}, 100 \times 10^{-5})$, which correspond respectively to a classical axially-loaded buckling mode, a mixed buckling mode, and a classical laterally-loaded buckling mode. This can also be validated by Figure 6 as the aforementioned.

5.2. Buckling under Axial and Torsional Combined-Load

Figures 8a–8f show the buckling modes under various λ_2. With the increase of λ_1, the buckling mode converts gradually from the classical axially loaded buckling mode characterized by $m = 8$ (see Figure 8a) to the classical torsional buckling mode characterized by $m = 1$ (see Figure 8f). Also, with the increase of λ_2, the axial half wave number m decreases and the torsional angel γ increases gradually. Although there is a slight γ seen in Figure 8b, the buckling is still dominated by axial

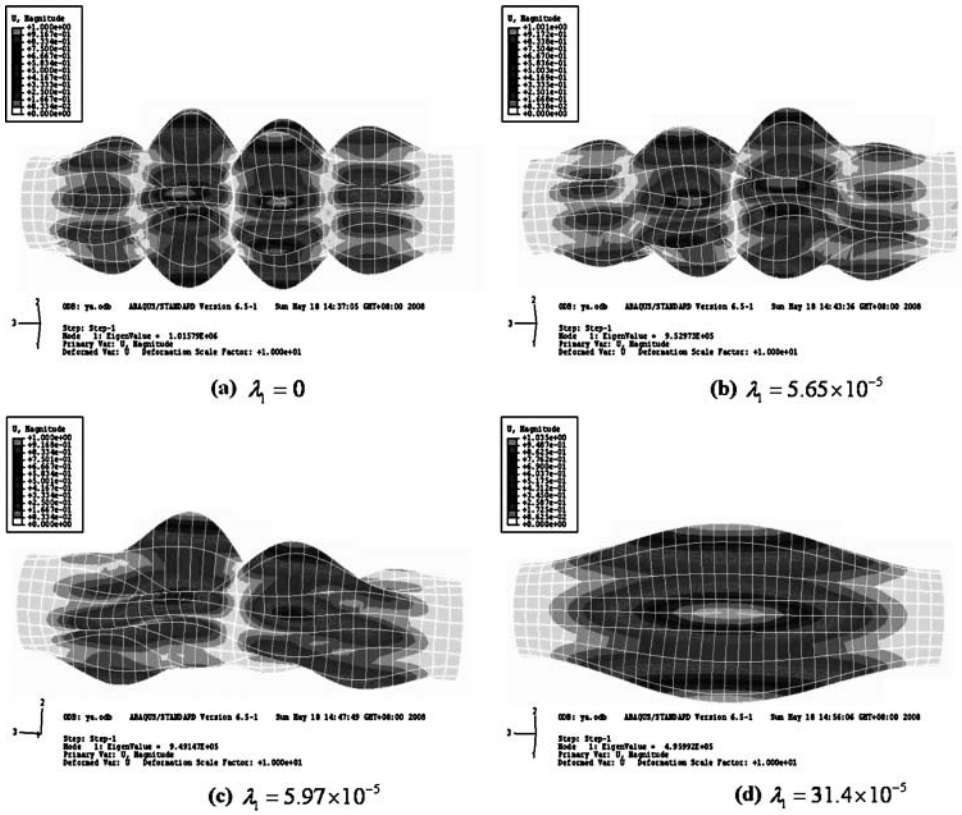

FIG. 6. Buckling modes of FGCSs under ALCC ($N = 1, l = 1m, R = 0.1m, h = 1mm$).

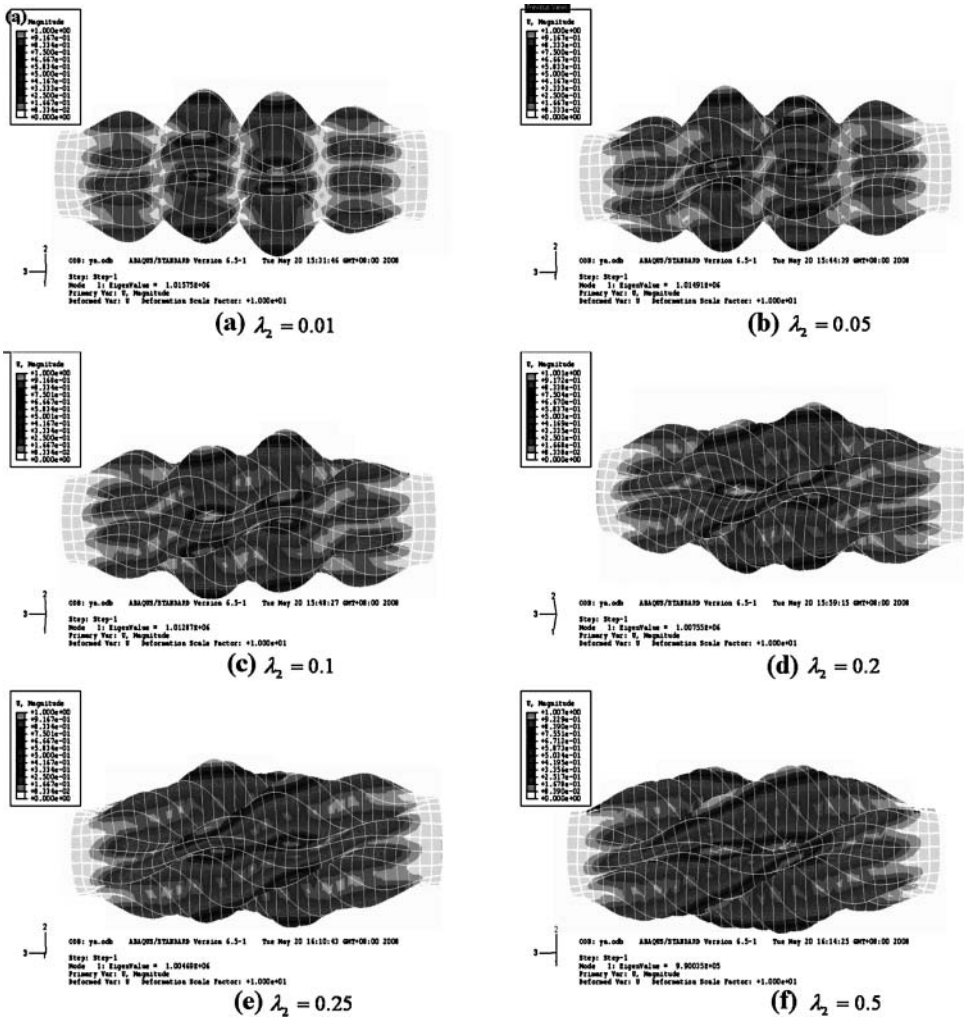

FIG. 8. Buckling modes of FGCSs under ATCC ($N = 1, l = 1m, R = 0.1m, h = 1mm$).

load. Figures 8c–8e show mixed buckling modes aroused by interaction between axial load and torsional load.

Figure 9 shows excellent agreement between theoretical results and FEM results. It is remarkable that, with the increase of λ_2, P_{cr} keeps nearly invariable and decreases slightly. Thus, the contributions of axial load and torsion load to buckling equate to each other and Figure 7 cannot be used to determine the load-dominant bounds as in the axial and lateral combined load case. However, one can determine the load-dominant bounds from Figure 8 where the value of λ_2 can be divided into three different regions according to the value of m, i.e., $(0, 0.050)$, $(0.05, 0.5)$, and $(0.5, +\infty)$, which correspond respectively to a classical axially-loaded buckling mode, a mixed buckling mode, and a classical torsional buckling mode.

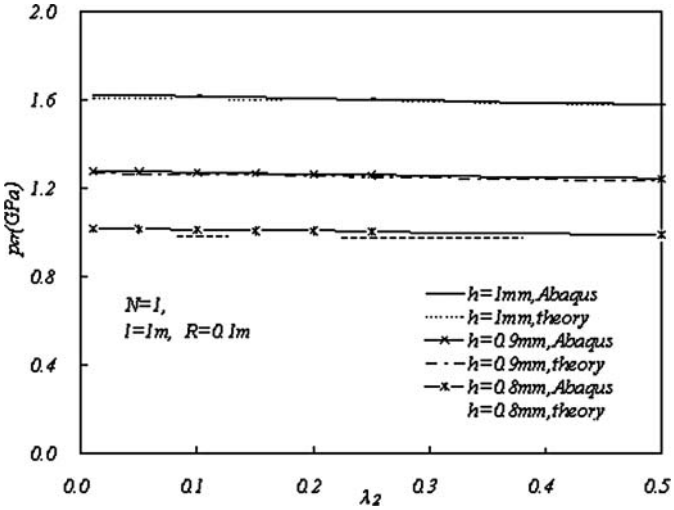

FIG. 9. Comparison of theoretical results with FEM results under ATCC.

5.3. Buckling under Lateral and Torsional Combined-Load

Figures 10a and 10b show the buckling modes under $\lambda_3 = 2 \times 10^8, 2 \times 10^9$. It is clear that, with the increase of λ_3, the

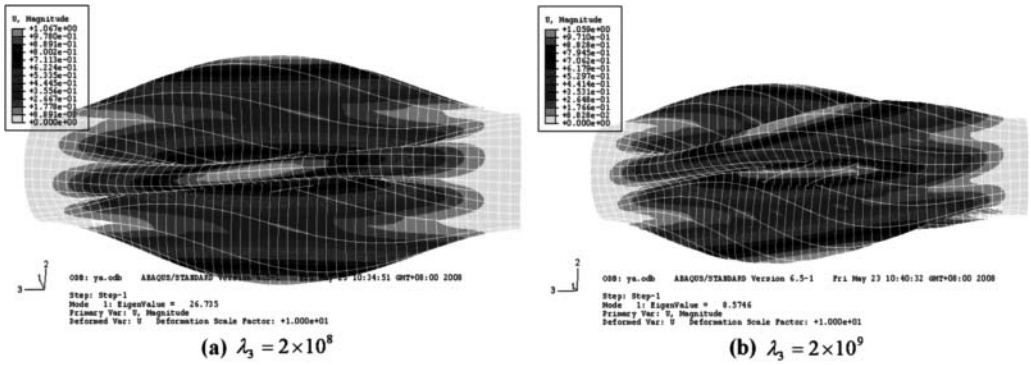

FIG. 10. Buckling modes of FGCSs under LTCC ($N = 1, l = 1m, R = 0.1m, h = 1mm$).

torsional angel γ enlarges. As the axial half wave number m under lateral and torsional loads are equated, i.e., $m = 1$, there is no character to determine the load-dominant bounds from Figure 10.

Figure 11 shows excellent agreement between theoretical results and FEM results. λ_3-axis is in the logarithmic form. It is remarkable that, with the increase of λ_3, there appears, in order, a slow, rapid, and then re-slow decrease of P_{cr}. This shows that buckling of the structure is more sensitive to lateral load than to torsional load, and the value of λ_3 can accordingly be divided into three different regions, i.e., $(0\ ,\ 2\times10^8]$, $(2\times10^8, 2\times10^{10})$, and $[2\times10^{10}\ ,\ +\infty)$, which correspond respectively to a classical laterally-loaded buckling mode, a mixed buckling mode, and a classical torsional buckling mode.

6. CONCLUSIONS

Buckling behaviors of combined-loaded FGCSs are investigated by using two different methods, the Ritz energy method and FEM. The combined-loads are composed of three relevant external forces, i.e., axial compression, lateral pressure, and torsion. Results of these two different methods are in excellent agreement, which validates the reliability of the present analysis. Theoretical and numerical results show that the contribution of lateral pressure to buckling of FGCSs is more significant than that of axial compression or torsion, while the contributions of axial compression and torsion are almost the same. Meanwhile, in a two-load combination case, either a single buckling mode due to one dominant load or a mixed buckling mode due to interaction of the two loads may appear according to the value of load ratio parameter. A practical method is proposed to determine the load-dominant bound between the single buckling mode and the mixed buckling mode, that is, in ALCC, the load-dominant bound can be determined from both the figure of different buckling modes and the relation curve of the critical load versus the load-ratio parameter, while in ATCC, it can be only determined from the figure of different buckling modes, and in LTCC, it can be only determined from the relation curve of the critical load versus the load-ratio parameter.

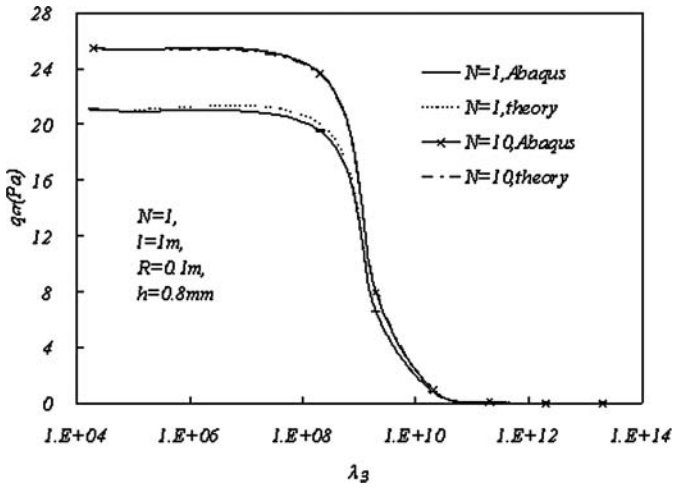

FIG. 11. Comparison of theoretical results with FEM results under LTCC.

ACKNOWLEDGMENTS

The authors wish to acknowledge support from the Natural Science Foundation of Guangdong Provin (10151064101000062) and the China Postdoctoral Science Foundation (20100470912) and the Fundamental Research Funds for the Central Universities, SCUT (2009ZM0054).

REFERENCES

1. M. Koizumi, The Concept of FGM, Ceramic Trans., vol. 34, pp. 3–10, 1993.
2. N. Noda, Thermal Stresses in Functionally Graded Materials, J. Therm. Stresses, vol. 22, pp. 477–512, 1999.
3. Y.M. Shabana, and N. Noda, Combined Macroscopic and Microscopic Analysis of Thermoelastoplastic Stresses of a Functionally Graded Material Plate, J. Therm. Stresses, vol. 24, pp. 799–815, 2001.
4. K.S. Kim, and N. Noda, Green's Function Approach to Unsteady Thermal Stresses in an Infinite Hollow Cylinder of Functionally Graded Material, Acta Mechanica, vol. 156, p. 145, 2002.
5. J.N. Reddy, and C.D. Chin, Thermoelastical Analysis of Functional Graded Cylinders and Plates, J. Therm. Stresses, vol. 21, pp. 593–626, 1998.
6. G.N. Praveen, and J.N. Reddy, Nonlinear Transient Thermoelastic Analysis of Functionally Graded Ceramic-Metal Plates, Int. J. Solids & Struct., vol. 35, pp. 4457–4476, 1998.

7. J. Aboudi, M.J. Pindera, and S.M. Arnold, Thermoelastic Theory for the Response of Materials Functionally Graded in Two Directions, Int. J. Solids & Struct., vol. 33, pp. 931–966, 1996.
8. C.T. Loy, K.Y. Lam, and J.N. Reddy, Vibration of Functionally Graded Cylindrical Shells, Int. J. Mech. Sci., vol. 41, pp. 309–324, 1999.
9. R.K. Bhangale, and N. Ganesan, Free Vibration Studies of Simply Supported Non-Homogeneous Functionally Graded Magneto-Electro-Elastic Finite Cylindrical Shells, J. Sound & Vibration, vol. 288, pp. 412–422, 2005.
10. T.Y. Ng, K.Y. Lam, K.M. Liew, and J.N. Reddy, Dynamic Stability Analysis of Functionally Graded Cylindrical Shells under Periodic Axial Loading, Int. J. Solids & Struct., vol. 38, pp. 1295–1309, 2001.
11. M. Darabi, M. Darvizeh, and A. Darvizeh, Non-Linear Analysis of Dynamic Stability for Functionally Graded Cylindrical Shells under Periodic Axial Loading, Compos. Struct., vol. 83, pp. 201–211, 2008.
12. R. Shahsiah, and M.R. Eslami, Thermal Buckling of Functionally Graded Cylindrical Shell, J. Therm. Stresses, vol. 26, pp. 277–294, 2003.
13. L. Wu, Z.Q. Jiang, and J. Liu, Thermoelastic Stability of Functionally Graded Cylindrical Shells, Compos. Struct., vol. 70, pp. 60–68, 2005.
14. R. Kadoli, and N. Ganesan, Buckling and Free Vibration Analysis of Functionally Graded Cylindrical Shells Subjected to a Temperature-Specified Boundary Condition, J. Sound & Vibration, vol. 289, pp. 450–480, 2006.
15. S.L. Li, and R.C. Batrab, Buckling of Axially Compressed Thin Cylindrical Shells with Functionally Graded Middle Layer, Thin-Walled Struct., vol. 44, pp. 1039–1047, 2006.
16. M.M. Najafizadeh, A. Hasani, and P. Khazaeinejad, Mechanical Stability of Functionally Graded Stiffened Cylindrical Shells, Appl. Math. Model., vol. 33, pp. 1151–1157, 2009.
17. A.H. Sofiyev, Dynamic Buckling of Functionally Graded Cylindrical Thin Shells under Non-Periodic Impulsive Loading, Acta Mechanica, vol. 165, pp. 151–163, 2003.
18. A.H. Sofiyev. The stability of compositionally graded ceramic–metal cylindrical shells under aperiodic axial impulsive loading, Compos. Struct., vol. 69, pp. 247–257, 2005.
19. A.H. Sofiyev, and E. Schnack, The Stability of Functionally Graded Cylindrical Shells under Linearly Increasing Dynamic Torsional Loading, Eng. Struct., vol. 26, pp. 1321–1331, 2004.
20. H.S. Shen, Postbuckling Analysis of Axially-Loaded Functionally Graded Cylindrical Shells in Thermal Environments, Comp. Sci. & Tech., vol. 62, pp. 977–987, 2002.
21. H.S. Shen, Postbuckling Analysis of Pressure-Loaded Functionally Graded Cylindrical Shells in Thermal Environments, Eng. Struct., vol. 25, pp. 487–497, 2003.
22. H.S. Shen, and N. Noda, Postbuckling of FGM Cylindrical Shells under Combined Axial and Radial Mechanical Loads in Thermal Environments, Int. J. Solids & Struct., vol. 42, pp. 4641–4662, 2005.
23. N. Yamaki, Elastic Stability of Circular Cylindrical Shells. North-Holland Press, New York, pp. 383–452, 1984.
24. H.S. Shen, Postbuckling of Shear Deformable Cross-Ply Laminated Cylindrical Shells under Combined External Pressure and Axial Compression, Intl. J. Mech. Sci., vol. 43, pp. 2493–2523, 2001.
25. H.S. Shen, and Y. Xiang. Buckling and post-buckling of anisotropic laminated cylindrical shells under combined axial compression and torsion, Compos. Struct., vol. 84, pp. 375–386, 2008.
26. L.Y. Wu, Stability Theory of Plates and Shells (in Chinese). Huazhong University of Science and Technology (HUST) Press, Wuhan, pp. 123–139, 1996.
27. G. Gerard, Introduction to Structural Stability Theory. McGraw-Hill, New York, p. 170, 1962.
28. Z.G. Yang, Z. Zhong, and Y. Dai, Three Dimensional Elasticity Analysis of a Functionally Graded Rectangular Plate, Chinese Quart. Mech., vol. 20, pp. 206–511, 2004.
29. J.B. Liu, Three Dimensional Elasticity Analysis of Functionally Graded Thick Plates, J. Anhui Inst. Architec. & Indus., vol. 14, pp. 4–7, 2006.